Electronic Supplementary Material (ESI) for Sustainable Energy & Fuels.

Supporting Information

Polyhedral oligomeric silsesquioxane as a recyclable soft template to synthesize mesoporous polymeric carbon nitride with enhanced photocatalytic hydrogen evolution

Zhiwei Liang, Lei Liu,* Xiaojia Zhuang, Zicheng Tang, Haiping Li* and Wenbing Kang*

National Engineering Research Center for Colloidal Materials, School of Chemistry and Chemical Engineering, Shandong University, Jinan, Shandong, 250100, China

*Email: thuliulei@163.com (L. Liu);
hpli@sdu.edu.cn (H. Li);
wbkang@sdu.edu.cn (W. Kang)

S1. Experimental section

S1.1. Materials

Octamethyl-polyhedral oligomeric silsesquioxane (mPOSS) was purchased from Sigma. Melamine (99.0%), poly(3,4-ethylenedioxythiophene)-poly(styrenesulfonate) (PEDOT-PSS, 1.5 wt% in H_2O), chloroplatinic acid hexahydrate (99.95%), and triethanolamine (99.5%) were bought from Aladdin (China). All the chemicals were used as received.

S1.2. Preparation of M-CN

The mPOSS (0.6 g, the optimized amount by comparing photocatalytic H_2 evolution rates of products (Fig. S1)) was dispersed in DMF (100 mL) by sonification for 30 min. Then, melamine (2.0 g) was added into the dispersion and the dispersion was evaporated at 80 °C under stirring until completely dried. The obtained solid was dried at 60 °C for 24 h in an oven, and put in a crucible with a lid and heated at 550 °C for 4 h in the N_2 atmosphere with a temperature ramp of 5 °C/min. After cooling naturally to the room temperature, the sample was dispersed in H_2O (100 mL) and stirred for 2 h. After filtration, washing with water, and drying at 60 °C for12 h, the product with slight silica residue was gained. To completely remove the residual silica in the product, the product was dispersed in the NH_4HF_2 solution (4 M, 50 mL) and stirred for 24 h. After filtration, washing with water and ethanol for several times, and drying at 60 °C for 12 h, the final yellow product, marked as M-CN, was obtained. For comparison, the bulk CN was prepared by direct calcination of melamine via a similar route without using mPOSS.

S1.3. Characterizations

Powder X-ray diffraction (XRD) patterns were measured at the room temperature with a Rigaku smart apparatus with Cu Kα radiation (λ = 1.54056 Å). X-ray photoelectron spectroscopy (XPS) was carried out on a Thermo Scientific Escalab 250Xi spectrometer (UK) with Al Kα radiation. The binding energies of all the peaks were corrected by that of the C 1s peak (284.6 eV). Morphologies of samples were observed on a Zeiss Supra55 field emission-scanning electron microscope (SEM, Germany) equipped with an energy dispersive X-ray spectrometer (EDS) and on a Jeol JEM-2100F transmission electron microscope (TEM, Japan). UV-Vis diffuse reflectance spectroscopy (DRS) was performed on a U-3900H spectrophotometer (Hitachi, Japan). Thermal analysis was performed on a TGA5500 thermogravimetric analyzer (TA, USA) in the N_2 atmosphere with a heating rate of 10 °C min^{-1}. Photoluminescence (PL) spectra were measured using a Hitachi F-7100 spectrophotometer (Japan) with an excitation wavelength of 380 nm, and excitation and emission slit widths of 5 nm, respectively. Time-resolved fluorescence decay spectra were recorded on an FLS920 time-resolved spectrofluorometer (Edinburgh Analytical Instruments, UK), with excitation and monitoring wavelength of 375 and 465 nm, respectively. A triple exponential model, [1] $I(t) = \sum_{i=1}^{i=3} B_i e^{-t/\tau_i}$ where I, τ_i and B_i are the intensity, the fluorescence lifetime and the amplitude of the i_{th} component, respectively, was used to fit the decay curves. N_2 sorption isotherms were measured on a Micromeritics TriStar II 3020 instrument (USA) at liquid nitrogen temperature. Samples were degassed at 150 °C for 3 h under vacuum before measurement. Solid-state ^{29}Si nuclear magnetic resonance (NMR) spectrometry was carried out on a Bruker AVANCE III 600 spectrometer with sodium 3-(trimethylsilyl) propane-1-sulfonate (DSS) as the reference substance. Fourier transform infrared (FT-IR) spectra were tested on a Bruker Tensor 27 spectrophotometer. Elemental analysis was performed on a Vario EL Cube (Elementar, Germany).

S1.4. Photoelectrochemical tests

Photoelectrochemical tests were performed on a CHI660E electrochemical workstation (Chenhua, China) with a standard three-electrode system soaked in the 0.2 M Na_2SO_4 solution. Ag/AgCl and Pt wire were used as reference and counter electrodes, respectively. The working electrode was obtained by dip-coating photocatalyst slurry on the ITO glass, followed by dried at 60 °C for 24 h and calcined at

200 °C for 2 h in N_2 atmosphere. The slurries were obtained by grinding mixtures of 0.02 g of photocatalyst, 40 μL of PEDOT-PSS, and 400 μL of H_2O. For photocurrent density, the applied bias is –0.3 V. A 300 W Xe-lamp (PLS-SXE300D, Beijing Perfectlight Technology Co., Ltd., China) with a UV-cut off filter ($\lambda \geq 420$ nm) was used as the light source. For Mott-Schottky plot tests, selected frequencies are 1.5 and 2.0 kHz; ethanol (800 μL) and ethylene glycol (200 μL) were substituted for PEDOT-PSS and H_2O for slurry preparation; and the 0.1 M KCl electrolyte containing 2.5 mM $K_3Fe(CN)_6$ and 2.5 mM $K_4Fe(CN)_6$ was substituted for the 0.2 M Na_2SO_4 electrolyte.

S1.5. Photocatalytic performance measurement

The photocatalytic H_2 evolution rate from water splitting was used to assess the photocatalytic activity of samples. All the photocatalytic experiments were done on a Labsolar-6A full glass automatic on-line trace gas analysis system (Perfectlight) connected with a closed-cycle gas circulation system. The photocatalyst powder (20 mg) was dispersed in triethanolamine (TEOA) aqueous solution (10 vol %, 100 mL) and then the Pt cocatalyst (3 wt %) was deposited on the surface of the photocatalyst by using an in-situ photoreduction method with H_2PtCl_6 as a precursor. The reactant solution was evacuated several times to remove air completely before irradiation under a 300 W Xe-lamp (PLS-SXE300D, Perfectlight) with a UV-cut off filter ($\lambda \geq 420$ nm). The temperature of the reaction solution was controlled at 20 °C by a flow of cooling water. The generated hydrogen was analyzed by gas chromatography equipped with a thermal conductive detector (TCD) and a 5 Å molecular sieve column, using argon as the carrier gas. For measurement of the apparent quantum yield (AQY), a THORLABs FB420-10 band-pass filter (λ = 420±2 nm) was substituted for above-mentioned UV-cut off filter. Average irradiation intensity (E) and the irradiation area (A) of the light are 3.82 mW cm^{-2} and 3.46 cm^2, respectively. Then, AQY was calculated by the equation, AQY = $(2hcN_A \cdot r_H)/(EA\lambda) \times 100\%$ where h, c, N_A, and r_H, are the Planck constant (6.626×10^{-34} J s), the light rate (3.0×10^8 m s^{-1}), the Avogadro's constant (6.02×10^{23} mol^{-1}), and the H_2 evolution rate (mol s^{-1}), respectively.

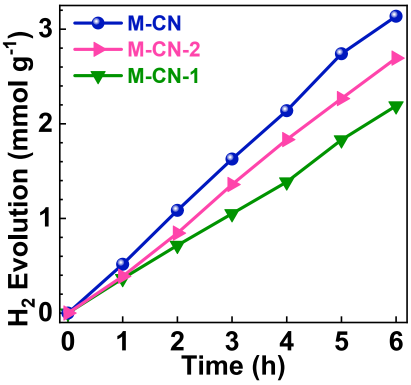

Fig. S1 Photocatalytic H_2 evolution on various samples.

M-CN-1 and M-CN-2 were synthesized by a similar way as M-CN (Section 1.2), except that the added mPOSS amount is 0.5 and 0.7 g, respectively. As shown in Fig. S1, M-CN exhibits the highest photocatalytic activity.

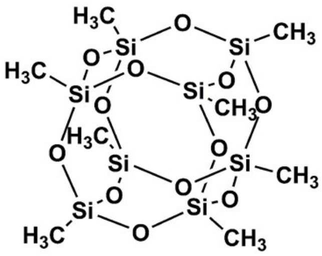

Fig. S2 The molecular structure of mPOSS.

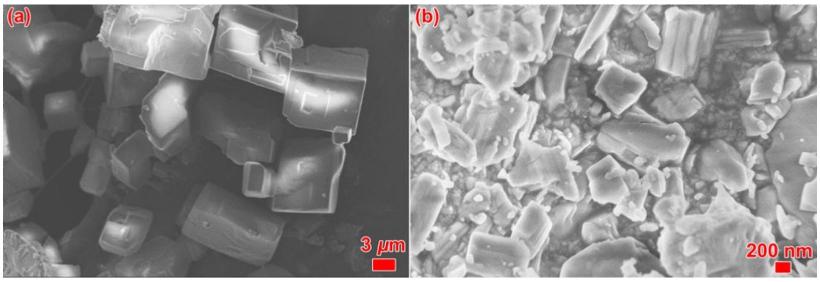

Fig. S3 SEM images of mPOSS.

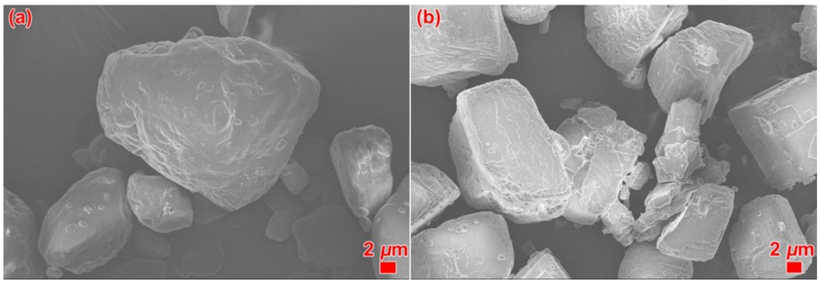

Fig. S4 SEM images of (a) melamine and (b) the mixture of melamine and mPOSS.

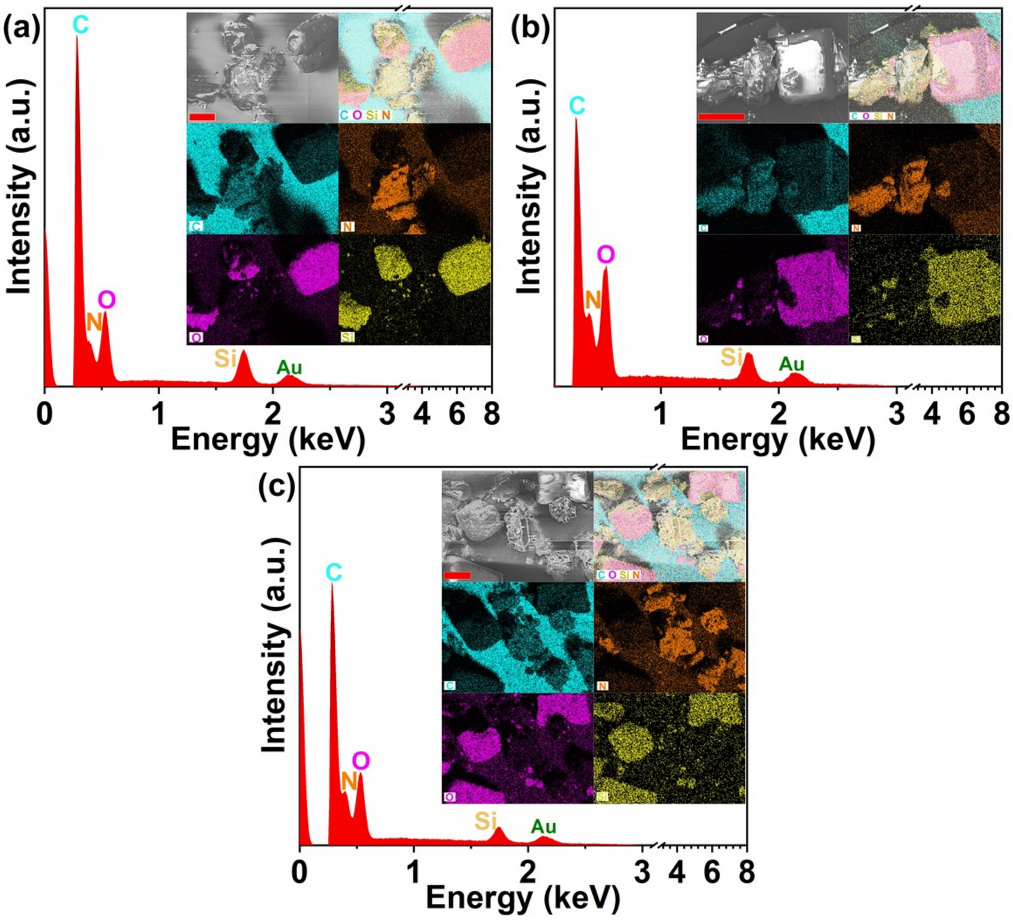

Fig. S5 EDS spectra of the mixture of melamine and mPOSS. Insets in the figure are corresponding elemental mapping images. Au is the conductive agent and conductive resin containing C and O was used as the adhesive for EDS tests. Scale bar: 10 μm.

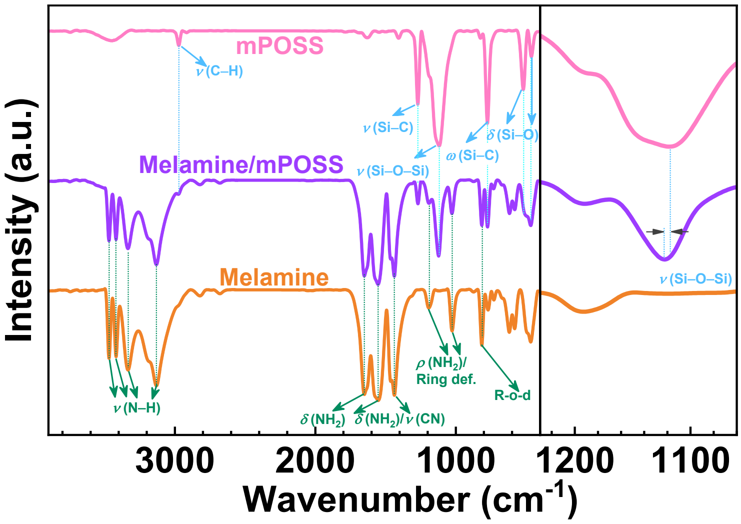

Fig. S6 FT-IR spectra of different samples. "R-o-d" means ring out-of-plane deformation.

As shown in Fig. S6, the absorption bands of both melamine and mPOSS can be observed in their mixture, indicating their molecular structures are stable in the mixing process, but the Si–O–Si peak of mPOSS at 1118 cm^{-1} shifts to 1123 cm^{-1} for the mixture, suggesting the hydrogen bonding interaction [2] between O atoms in mPOSS and –NH_2 in melamine.

Table S1 Absorption bands of melamine [3] and mPOSS. [4]

Sample	Absorption band (cm^{-1})	Vibration
Melamine	3486–2895	N–H stretching
	~1653	NH_2 bending
	1583 and 1550	NH_2 bending and C–N stretching
	1464 and 1437	NH_2 bending and C–N stretching
	1190 and 1023	NH_2 and ring deforming
	814	ring out-of-plane deforming
mPOSS	3435	Si–OH stretching
	2976	C–H stretching
	1630	H_2O bending
	1264	Si–C stretching
	1118	Si–O–Si stretching
	769	Si–C wagging
	512 and 460	Si–O bending

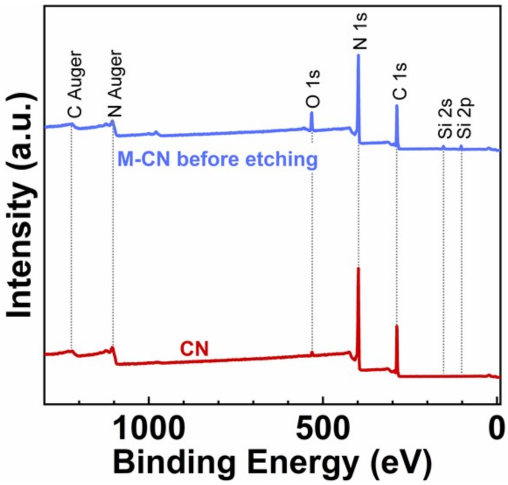

Fig. S7 Survey XPS spectra of CN and M-CN before etching.

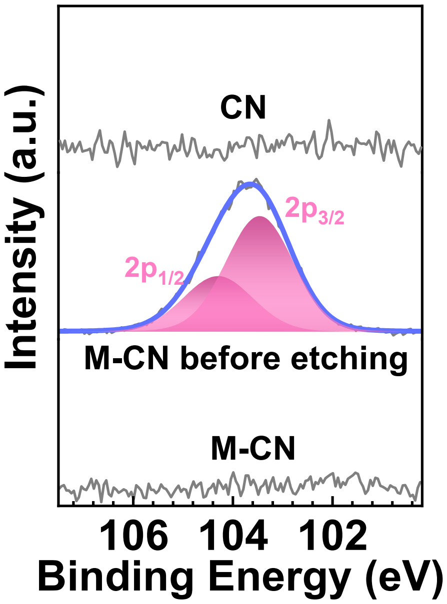

Fig. S8 Si 2p core-level XPS spectra of CN, M-CN before etching and M-CN.

As shown in Fig. S8, the binding energy at 104.3 and 103.5 eV for M-CN before etched by NH_4HF_2 corresponds to $2p_{1/2}$ and $2p_{3/2}$ peaks of Si atoms in the inorganic silica-like phase. [5, 6] After the etching of NH_4HF_2, there is no silica residue in M-CN any more. According to the XPS data, the residual silica content in the product is ~5 wt%.

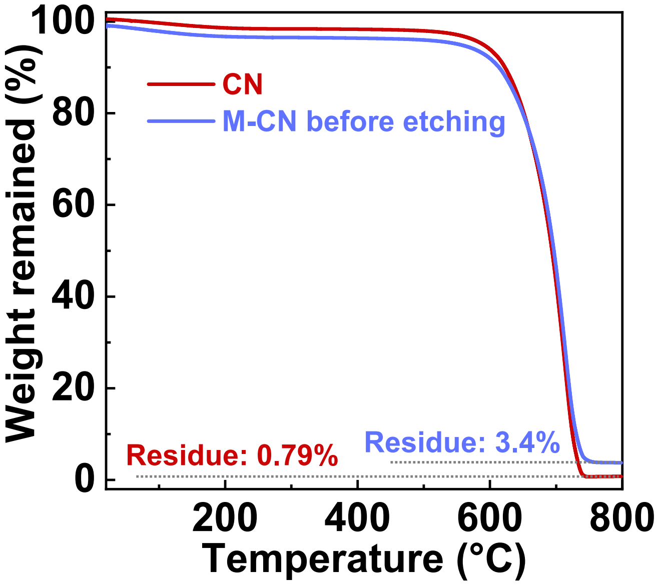

Fig. S9 Thermogravimetric analysis (TGA) curves of CN and M-CN.

As shown in Fig. S9, more residue in M-CN before etching than that in the bulk CN suggests the existence of silica in the former. And the residual silica content in the product is <3 wt%.

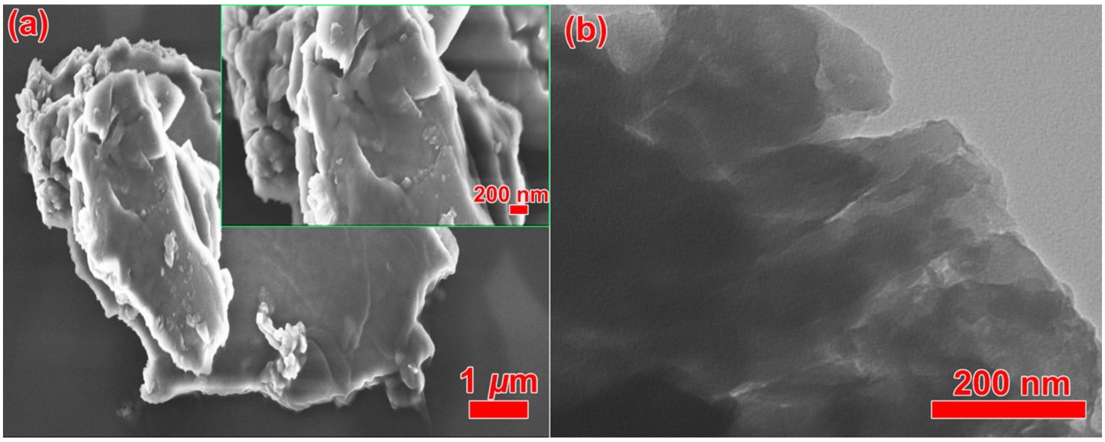

Fig. S10 (a) SEM and (b) TEM images of the bulk CN. Insets in (a) are enlarged images.

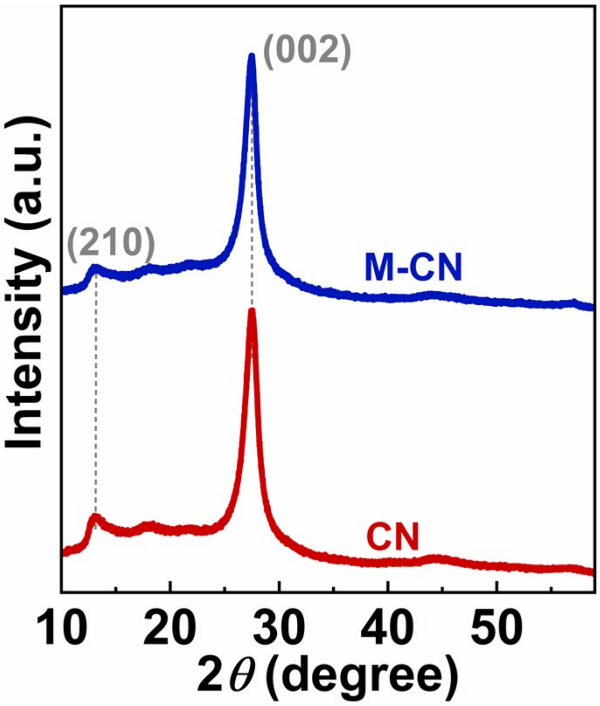

Fig. S11 XRD patterns of CN and M-CN.

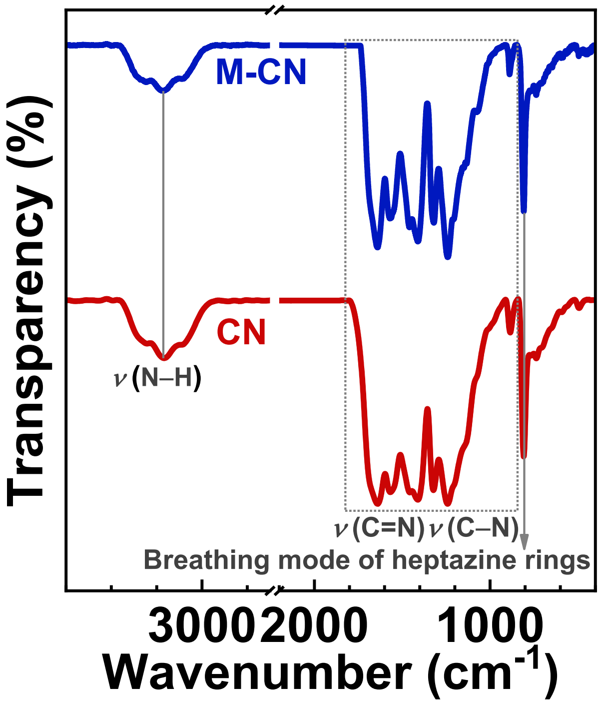

Fig. S12 FT-IR spectra of CN and M-CN.

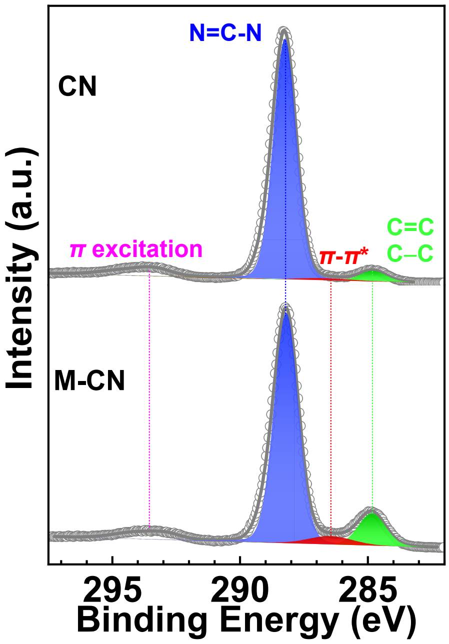

Fig. S13 C 1s core-level XPS spectra of CN and M-CN.

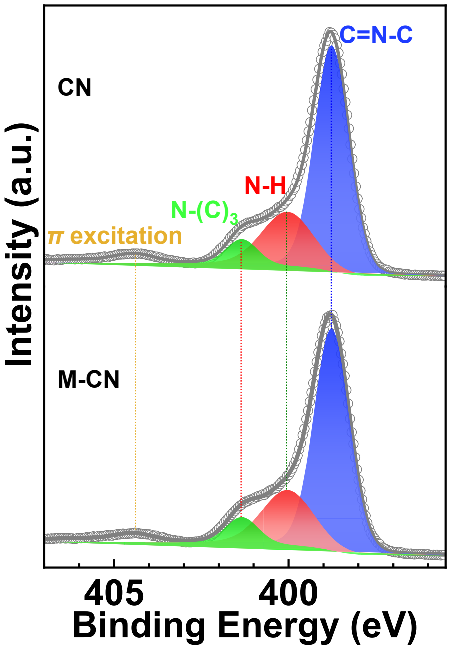

Fig. S14 N 1s core-level XPS spectra of CN and M-CN.

Table S2 Elemental analysis data of CN and M-CN.

Sample	N (wt%)	C (wt%)	H (wt%)	Molar ratio of N/C
CN	61.51	35.13	1.79	1.50
M-CN	60.09	34.38	1.83	1.50

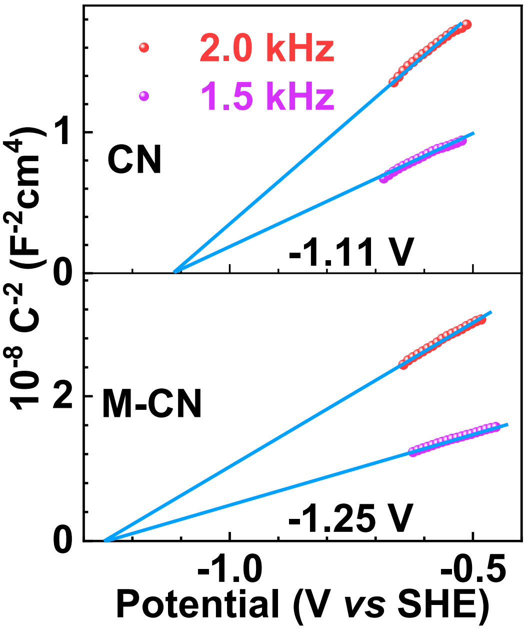

Fig. S15 Mott-Schottky plots of CN and M-CN.

As shown in Fig. S15, the positive slopes of the extensive lines in the figure indicate that the samples are n-type semiconductors. [7] For n-type semiconductors, the flat potentials determined in the figure are approximately equal to the conduct band minimum. [8]

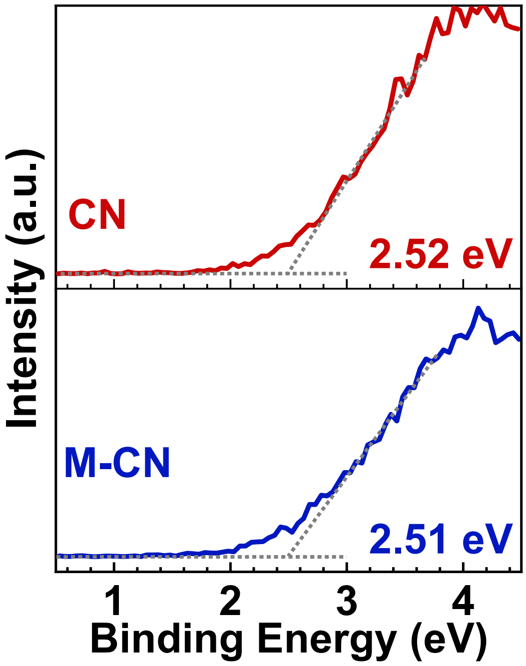

Fig. S16 VB-XPS spectra of CN and M-CN.

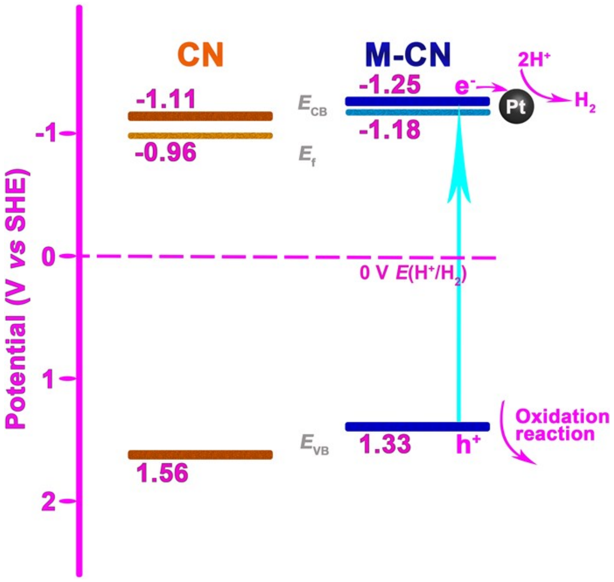

Fig. S17 Energy band levels of CN and M-CN.

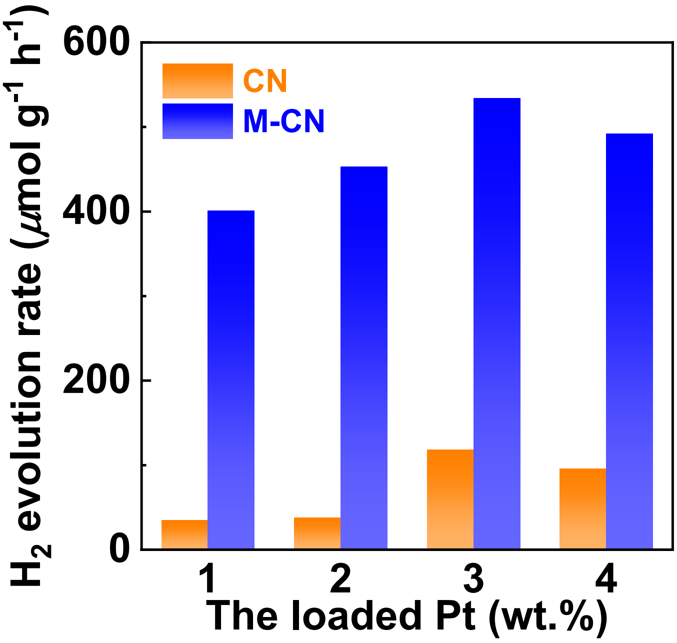

Fig. S18 Photocatalytic hydrogen evolution on CN and M-CN with various Pt loading amount and 10 vol% TEOA as the electron donor, under visible light irradiation ($\lambda > 420$ nm).

Table S3. Photocatalytic H_2 evolution activity and basic experimental conditions of reported template-synthesized mesoporous CN photocatalysts.

Photocatalyst	Cocatalyst	Sacrificial agent	Light source	R_H [b]	AQY(%) at 420 nm	Ref.
M-CN	3 wt% Pt	TEOA [a] (10 vol%)	300-W Xe lamp ($\lambda > 420$ nm)	**534**	**2.0**	**This work**
Sulfur-mediated g-C_3N_4	1.5 wt% Pt	TEOA (10 vol%)	300-W Xe lamp ($\lambda > 400$ nm)	501	\	[9]
Worm-like g-C_3N_4	0.5 wt% Pt	TEOA (10 vol%)	300-W Xe lamp ($\lambda > 420$ nm)	494	1.8	[10]
Cl-g-C_3N_4	3 wt% Pt	Lactic acid (33 vol%)	300-W Xe lamp ($\lambda >$ 420 nm)	537	11.9	[11]
Honeycomb-like structured g-C_3N_4	3 wt% Pt	Lactic acid (25 vol%)	300-W Xe lamp ($\lambda > 400$ nm)	459	2.2	[12]
Mesoporous g-C_3N_4	Pt	TEOA (10 vol%)	500-W HBO lamp (λ> 420 nm)	850	\	[13]
……		……	……	……		……

[a] Triethanolamine; [b] photocatalytic hydrogen evolution rate (μmol g^{-1} h^{-1})

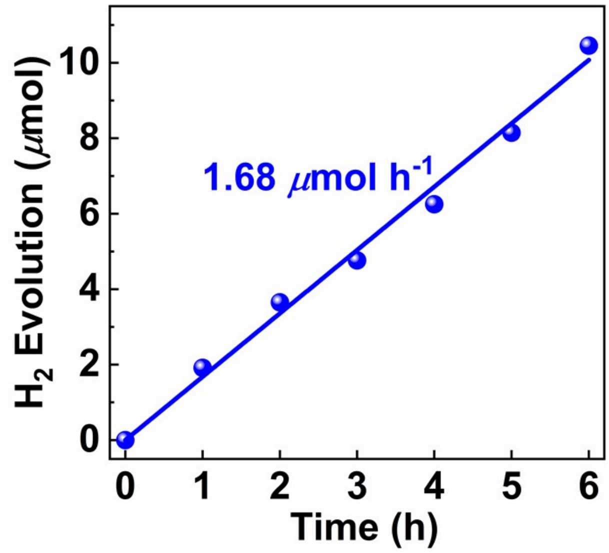

Fig. S19 Photocatalytic hydrogen evolution on M-CN with 3 wt% Pt as the cocatalyst and 10 vol% TEOA as the electron donor, under irradiation of 420-nm light.

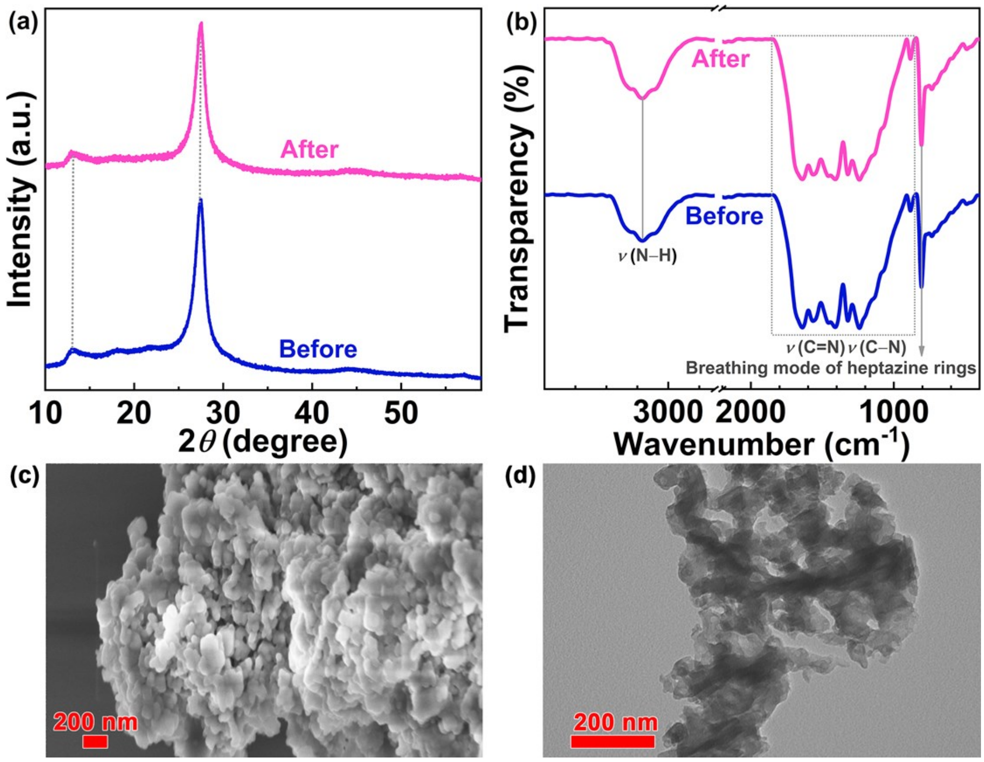

Fig. S20 (a) XRD patterns and (b) FT-IR spectra of M-CN before and after the cyclic H_2 evolution experiments; and (c) SEM and (d)TEM images of M-CN after the cyclic experiments.

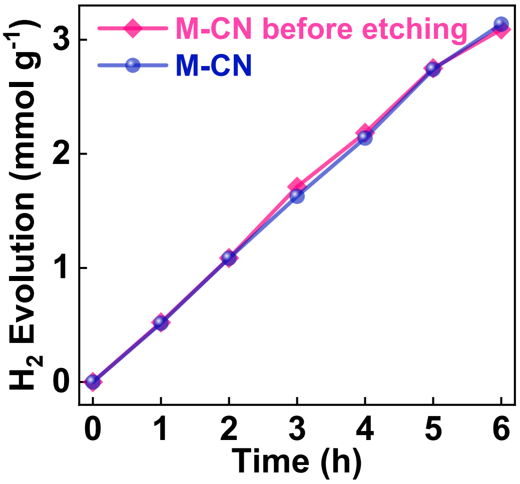

Fig. S21 Photocatalytic H_2 evolution on the samples with Pt as the cocatalyst and 10 vol% TEOA as the electron donor, under visible light irradiation.

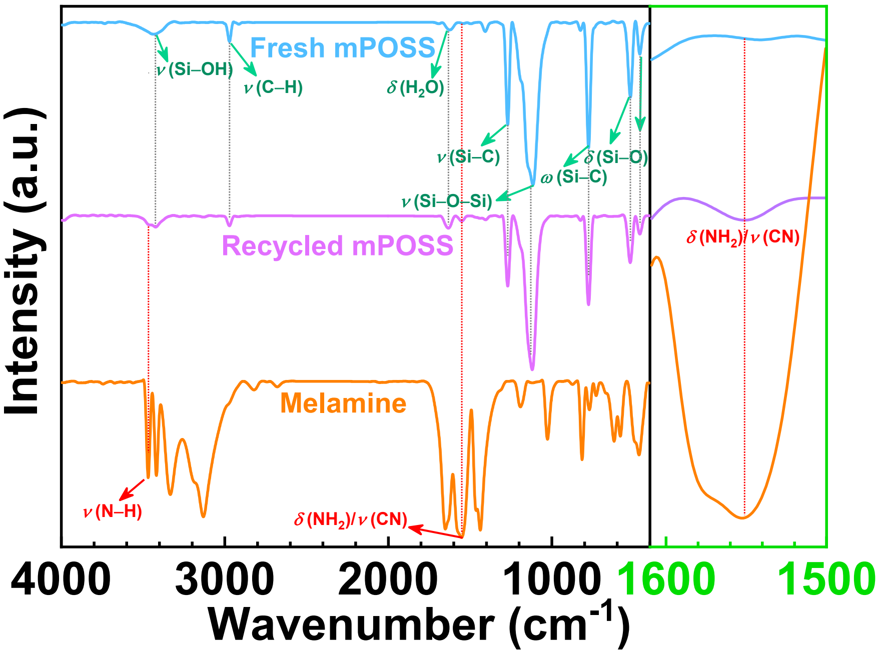

Fig. S22 FT-IR spectra of melamine, fresh and recycled mPOSS.

As shown in Fig. S22, the FT-IR spectrum of the recycled mPOSS shows similar absorption bands as that of the fresh one, apart from the weak absorption bands of melamine at ~3468 cm^{-1}, ascribed to N–H stretching vibration, and ~1550 cm^{-1}, ascribed to NH_2 bending and C–N stretching vibrations, respectively (see Table S1).

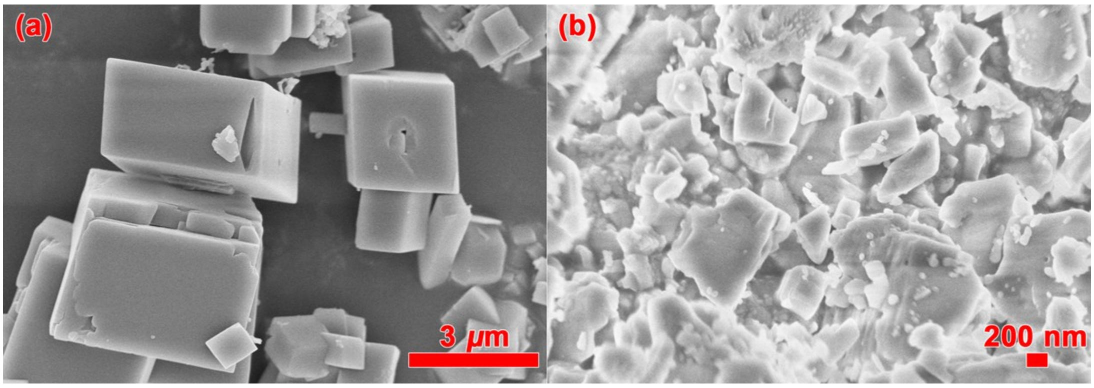

Fig. S23 SEM images of the recycled mPOSS.

References

1. R. Godin, Y. Wang, M. A. Zwijnenburg, J. Tang and J. R. Durrant, *J. Am. Chem. Soc.*, 2017, **139**, 5216-5224.
2. M. S. Islam, W. S. Choi and H.-J. Lee, *ACS Appl. Mater. Interfaces*, 2014, **6**, 9563-9571.
3. N. E. Mircescu, M. Oltean, V. Chiş and N. Leopold, *Vib. Spectrosc*, 2012, **62**, 165-171.
4. E. S. Park, H. W. Ro, C. V. Nguyen, R. L. Jaffe and D. Y. Yoon, *Chem. Mater.*, 2008, **20**, 1548-1554.
5. C.-H. Su, Y.-P. Chiu, C.-C. Teng and C.-L. Chiang, *J. Polym. Res.*, 2010, **17**, 673-681.
6. Y. R. Liu, Y. D. Huang and L. Liu, *Polym. Degrad. Stab.*, 2006, **91**, 2731-2738.
7. Z. Liang, Y. Xia, G. Ba, H. Li, Q. Deng and W. Hou, *Catal. Sci. Technol.*, 2019, **9**, 6627-6637.
8. G. Zhang, Z.-A. Lan, L. Lin, S. Lin and X. Wang, *Chem. Sci.*, 2016, **7**, 3062-3066.
9. F. He, G. Chen, Y. Yu, Y. Zhou, Y. Zheng and S. Hao, *Chem. Commun.*, 2015, **51**, 425-427.
10. H. Yan, *Chem. Commun.*, 2012, **48**, 3430-3432.

11. C. Liu, Y. Zhang, F. Dong, A. H. Reshak, L. Ye, N. Pinna, C. Zeng, T. Zhang and H. Huang, *Appl. Catal., B*, 2017, **203**, 465-474.
12. F. Yang, D. Liu, Y. Li, L. Cheng and J. Ye, *Appl. Catal., B*, 2019, **240**, 64-71.
13. X. Chen, Y.-S. Jun, K. Takanabe, K. Maeda, K. Domen, X. Fu, M. Antonietti and X. Wang, *Chem. Mater.*, 2009, **21**, 4093-4095.